Available online at www.sciencedirect.com
SCIENCE DIRECT
Polymer 45 (2004) 7779–7790
polymer
www.elsevier.com/locate/polymer

Network model for the viscoelastic behavior of polymer nanocomposites

Alireza S. Sarvestani*, Catalin R. Picu

Department of Mechanical, Aerospace and Nuclear Engineering, Rensselaer Polytechnic Institute, Troy, NY 12180, USA

Received 26 April 2004; received in revised form 16 August 2004; accepted 18 August 2004
Available online 15 September 2004

Abstract

A theoretical network model reproducing some significant features of the viscoelastic behavior of unentangled polymer melts reinforced with well dispersed non-agglomerated nanoparticles is presented. Nanocomposites with low filler volume fraction ($\sim$10%) and strong polymer–filler interactions are considered. The model is calibrated based on results obtained from discrete simulations of the equilibrium molecular structure of the material. This analysis provides the statistics of the network of chains connecting fillers, of dangling strands having one end adsorbed onto fillers, and that of the population of loops surrounding each nanoparticle. The network kinetics depends on the attachment–detachment dynamics of grafted chains of various types and is modeled by using a set of convection equations for the probability distribution functions. The overall viscoelastic response depends strongly on the lifetime of the polymer–filler junctions. The largest reinforcement is observed at low strain rates and low frequency oscillations. A solid like behavior is predicted for systems in which the polymer molecules interact strongly with the nanoparticles, effect which is associated with the behavior of the network of bridging segments.

Keywords: Polymer nanocomposites; Viscoelasticity; Transient networks

1. Introduction

Understanding and modeling the rheology of polymer composites consisting of particulates dispersed in polymer melts or concentrated solutions has received considerable attention. Despite these efforts, a comprehensive model able to predict the experimentally observed mechanical behavior is still not available. This situation is due to the complex microscopic interactions that control the macroscopic material response and to the evolution of the microstructure during deformation. In general, the flow characteristics of these systems depend on the properties of the two constituents, such as the size and shape of filler particles, their volume fraction, interparticle interactions, the molecular weight of the polymeric matrix and its viscosity, as well as on the nature of the polymer–filler interactions. In particular, understanding the relative importance of filler–filler and polymer–filler interactions, in conjunction with the contribution of hydrodynamic interactions is essential.

The interparticle interactions occur through electrostatic and van der Waals' forces and may result in the formation of particle aggregates and ultimately of fractal agglomerated structures [1–4]. The polymer–particle interactions refer to the attachment/detachment of chains to/from the filler surface, process controlled by the effective surface affinity [5–7]. The details of these thermodynamic interactions control the existence of either an adsorbed or a depleted polymer layer around each particle with presumably different dynamics compared to the bulk [8,9].

A broad understanding was developed over the years linking the nature of the filler–filler and polymer–filler interactions to experimentally observed phenomena such as the strain amplitude dependence of the complex dynamic moduli (Payne effect), solid like, yield like and thixotropic behavior, and frozen memory. In the case of strong filler–filler interactions, it is believed that the material response is greatly influenced by the evolution of the network of filler agglomerates and its break down and reformation during mechanical testing [3,10–12]. On the other hand, when the polymer–filler interactions dominate, it was shown experimentally that the nonlinear viscoelasticity of the suspension originates in the dynamics of the

* Corresponding author. Tel.: +1-518-276-8411; fax: +1-518-276-6025.
E-mail address: sarvea@rpi.edu (A.S. Sarvestani).

0032-3861/$ - see front matter © 2004 Elsevier Ltd. All rights reserved.
doi:10.1016/j.polymer.2004.08.060

stick-slip motion of polymeric chains on and close to the filler surface [13–15].

These generic conclusions and extensive experimental observations provided a basis for the development of constitutive equations for polymeric compounds. The early studies focused on the rheology of suspensions of hard spheres with exclusively hydrodynamic and Brownian interactions with the suspending fluid, subjected to small strains. The theory was gradually amended to include the effect of the filler shape (particles or aggregates), higher filler concentrations, complexity of suspending medium, and higher deformation rates [16–18]. The mechanism of hydrodynamic reinforcement of elastomers was studied, among others, by Huber and Vilgis [19].

When close-range filler–filler interactions dominate, phenomenological models of filler cluster breakdown and re-agglomeration cluster networks appear to be adequate to describe some aspects of the resulting nonlinear viscoelasticity [20]. Leonov [21] proposed a continuum thermodynamics approach for the kinetics of floc evolution, which was successful in describing yielding, thixotropy and frozen memory effects, without recurring to the use of a yield criterion. The case in which the filler–polymer interactions dominate was considered by Simhabhatla and Leonov [13] and by Havet and Isayev [22]. Maier and Göritz [23] proposed a phenomenological model for the Payne effect based solely on the interaction between fillers and polymeric chains.

In most existing analytical models, the dependence of the viscoelastic properties on filler size is not included. On the other hand, in many applications fillers with size comparable with the characteristic length scale of the suspending medium (e.g. the radius of gyration of polymeric chains) are used. In such situations, additional physics becomes important. The assumptions on which continuum viscoelasticity is based fail, while the validity of the Stokes–Einstein equation is controversial [24]. The situation is complicated by the fact that in nanocomposites, even at small filler volume fractions, a large surface area exists and most polymeric chains are at or close to a filler surface.

In order to clarify some of these issues, research efforts were recently directed toward investigating the molecular structure and dynamics of this type of composites by means of molecular simulations [9,25–27]. Mark and his collaborators performed a series of computer simulations on the elastomeric properties of reinforced rubbers (see Ref. [28] and references therein). These analyses provided significant insight, but a direct connection with the larger scale properties is still missing. The situation is due to the limitations of the current simulation capabilities to relatively short chains and short relaxation time spans. Longer (coarse grained) discrete simulations able to provide a larger fraction of the relaxation spectrum are possible, however, these include assumptions about the relevant physics at the smaller, unresolved scales.

In this paper we present a conceptual model for the overall viscoelasticity of polymer nanocomposites with strong filler–polymer interactions. We consider non-agglomerated configurations, in which rigid spherical nanoparticles with diameter comparable to the gyration radius of the host polymer molecules are homogeneously dispersed in the polymeric matrix. The structure of the polymer confined between nanofillers, as obtained from atomistic simulations, is presented in a separate publication [29]. There it is shown that, when the wall-to-wall distance between fillers becomes comparable to $2R_g$ (where R_g is the polymer radius of gyration), a network of polydisperse chain bridges linking neighboring fillers forms. Taking advantage of this insight, we develop a model attempting to reproduce the steady state viscoelasticity of the mixture. An example of a similar effort is given in Doremus and Piau [30]. The evolution of the internal structure of this multicomponent polymer system during deformation is represented using the conventional transient network theory [31] and the elastic dumbbell model with sticky ends [32]. The discrete simulation results for the equilibrium molecular structure [29] are used as initial conditions for the corresponding convection-diffusion equations. Consequently, a set of uncoupled nonlinear algebraic equations is developed to describe the steady state material response to an applied deformation rate. Numerical studies show that the lifetime of the polymer–particle junctions along with the non-Hookean behavior of chain segments have a significant influence on the material shear viscosity, especially at small deformation rates. The model also predicts a secondary plateau in the low frequency region for the linear dynamic response of composites with high polymer–particle affinity.

2. Theoretical model

The system studied here is composed of as an ensemble of linear unentangled monodisperse amorphous homopolymers and a random distribution of non-aggregated rigid spherical nanoparticles. The fillers are uniformly distributed in 3D with low concentration, on the order of 10 vol.%. The filler particle diameter and, hence, their average wall-to-wall distance are on the order of the polymer radius of gyration R_g at these volume fractions.

Fig. 1 shows schematically the internal chain-scale structure of the system. G, H, I, J, and K represent attachment points of a chain to two particles. Chain segments such as HI bridge fillers. A large number of polydisperse loops (e.g. GH, IJ, and JK) and dangling ends (e.g. GF) are attached to each filler. An isochoric, isothermal and homogeneous macro-deformation is applied to the system leading to the evolution of the molecular structure. Stress production and relaxation depend directly on this process.

In absence of topological entanglements, the molecular structure is modeled using a combination of the classical

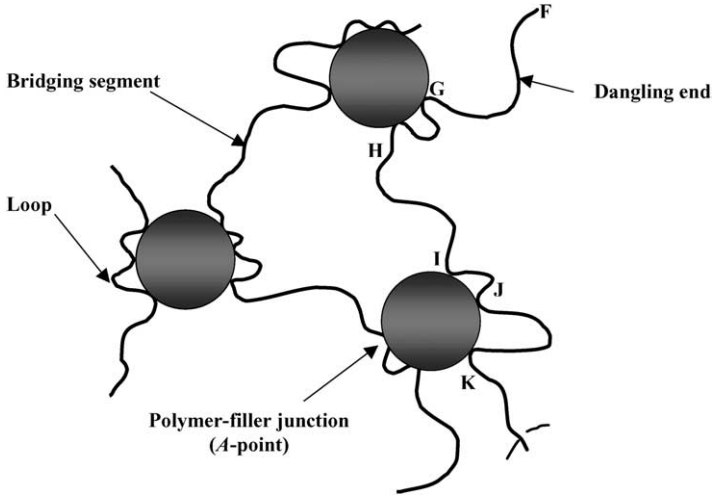

Fig. 1. Schematic representation of the molecular scale structure. The macromolecules are divided into networks bridging segments, as well as loops, and dangling ends.

network theory and the elastic dumbbell model for polydispersed polymer segments and localized junctions. A junction represents an adsorbed polymer–filler attachment (A-point). A segment can be a bridging segment, a loop, or a dangling end (Fig. 1). A-points are reversible junctions and their time evolution is due primarily to the applied deformation, but fluctuations are also possible in equilibrium. Hence, the destruction and creation of segments is also a stochastic reversible process. The internal structure has a transient topology and its dynamics is controlled by the rate of the attachment and detachment process and depends on the applied deformation.

Let us consider an arbitrary representative volume element. The end-to-end vector for a typical bridging or dangling segment is denoted by $\mathbf{R}$ (Fig. 2(a) and (b)). $\Psi_i^j(\mathbf{R}, t)$ is the distribution function of chain segments of type j. Here $j=B$ or $j=D$, where B stands for bridging segments and D refers to the dangling ends and loops. A loop of $2n$ monomers is visualized as two separate pseudo-dangling segments each of length n. i represents the number of 'beads' (Kuhn segments) in the respective chain segment. Hence, $\Psi_i^j(\mathbf{R}, t)\,\mathrm{d}\mathbf{R}$ represents the number density of strands of type j composed of i beads, having end-to-end vectors in the range $\mathrm{d}\mathbf{R}$ about $\mathbf{R}$. The total number density of this type of segments at time t is given by

$$N_i^j(t) = \int \Psi_i^j(\mathbf{R}, t)\mathrm{d}\mathbf{R}, \tag{1}$$

where the integration is performed over the end-to-end vector configuration space.

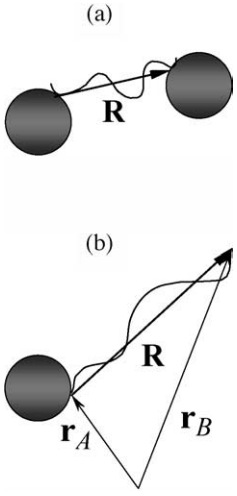

Fig. 2. End-to-end vector of a representative (a) bridging segment and (b) dangling end.

2.1. Evolution of bridging segments

Using the principle of local action, the time evolution of the distribution function for bridging segments is represented by the convection equation [31]

$$\frac{\partial \Psi_i^{\mathrm{B}}}{\partial t} = -\frac{\partial}{\partial \mathbf{R}} \cdot (\Psi_i^{\mathrm{B}} \dot{\mathbf{R}}) + G_i(\mathbf{R}, t) - D_i(\mathbf{R}, t), \tag{2}$$

where $G_i(\mathbf{R},t)$ and $D_i(\mathbf{R},t)$ represent the rate of generation and destruction of bridging segments per unit volume, respectively.

It is further assumed that the fillers move affinely with the applied macro-deformation. This assumption is supported by two observations: (a) a filler represents a node of the network. Since the effective coordination of this network is high (when the minimum wall-to-wall distance between fillers is on the order of R_g), according to the classical network theory, the nodes move affinely. The case in which the wall-to-wall distance is larger than $2R_g$ and a bridging network does not form is not discussed here. (b) The dense population of tethered chains provides significant friction with the surrounding medium, which promotes the affine deformation of fillers.

It results that the bridges follow the macroscopic deformation such that one may write (Fig. 2(a))

$$\dot{\mathbf{R}} = \mathbf{L}\cdot\mathbf{R}, \tag{3}$$

where $\mathbf{L}(t)$ is the macroscopic velocity gradient tensor. The tensor satisfies $\mathrm{tr}\,\mathbf{L}=0$, which represents the isochoric deformation assumption.

In general, there is no explicit form for the rate of generation and destruction functions in Eq. (2). These are described by phenomenological relations rooted in the linear response theory. For example, the bridge destruction function is often taken to be proportional to the current distribution, i.e. [33]

$$D_i(\mathbf{R},t) = d_i(R)\Psi_i^{\mathrm{B}}(\mathbf{R},t), \tag{4}$$

where $d_i(R)$ is the detachment probability for A-points, and therefore the probability of failure of bridging segments per unit time. Note that this quantity is considered a function of $R=|\mathbf{R}|$, as discussed in the next section.

The physical picture of the bridge formation rate is less obvious. It is usually considered that junction formation amounts to sampling the equilibrium distribution function of bridging segments [34]. However, it is physically more plausible to assume that the flow reduces the formation rate of junctions simply due to kinematic reasons [35,36]. Here, this effect is accounted for by including a term proportional to Ψ_i^{B} in the equation for the rate of bridge formation

$$G_i(\mathbf{R},t) = g_i(R)(\lambda_i^{\mathrm{B}}\Psi_{i,\mathrm{eq}}^{\mathrm{B}}(\mathbf{R}) - \Psi_i^{\mathrm{B}}(\mathbf{R},t)), \tag{5}$$

where $g_i(R)$ is the rate of A-point formation, and $\Psi_{i,\mathrm{eq}}^{\mathrm{B}}(\mathbf{R}) = \Psi_i^{\mathrm{B}}(\mathbf{R},0)$. λ_i^{B} is a dimensionless constant to be determined, which is included in order to keep the formulation consistent at time $t=0$ (in equilibrium). The discussion of the functional form of $d_i(R)$ and $g_i(R)$ is deferred to Section 3.

Substituting Eqs. (3)–(5) in Eq. (2), leads to an equation for the evolution of $\Psi_i^{\mathrm{B}}(\mathbf{R},t)$ of the form

$$\frac{\partial\Psi_i^{\mathrm{B}}}{\partial t} = -\frac{\partial}{\partial\mathbf{R}}\cdot(\mathbf{L}\cdot\mathbf{R}\Psi_i^{\mathrm{B}}) + g_i(R)(\lambda_i^{\mathrm{B}}\Psi_{i,\mathrm{eq}}^{\mathrm{B}}(\mathbf{R}) - \Psi_i^{\mathrm{B}}(\mathbf{R},t)) - d_i(R)\Psi_i^{\mathrm{B}}(\mathbf{R},t). \tag{6}$$

2.2. Evolution of terminal dangling segments

The dynamics of the end-to-end vector of dangling chains in the configuration space is represented by using a dumbbell model. Let us consider a dangling segment (Fig. 2(b)) attached to the representative filler at point A, its other end, point B, being free. The interaction with the matrix is represented through a frictional contact of the representative segment with the surrounding medium. The frictional force acts on the free end, while the attached end A is fixed. The dumbbell is elastic with no internal viscosity. In non-equilibrium, energy dissipation and stress relaxation occur as the strand relaxes toward the equilibrium configuration by a Brownian process. Thus, the dangling chains do not follow the deformation affinely. Let $\mathbf{r}_{\mathrm{A}}$ and $\mathbf{r}_{\mathrm{B}}$ represent the position vectors of the end points. We express the dynamics of the free end for a segment of i monomers, using a Langevin equation [31]

$$\varsigma_i\left(\frac{\mathrm{d}\mathbf{r}_{\mathrm{B}}(t)}{\mathrm{d}t} - \mathbf{L}(t)\cdot\mathbf{r}_{\mathrm{B}}(t)\right) = \mathbf{F}(\mathbf{r}_{\mathrm{B}}(t) - \mathbf{r}_{\mathrm{A}}(t)) + \mathbf{S}(t). \tag{7}$$

ς_i is the segmental friction coefficient which, as usual, is assumed to be configuration independent, $\mathbf{F}(t)$ is the attractive entropic force between the two ends, and $\mathbf{S}(t)$ is a random force. Further, we assume $\varsigma_i \approx i\varsigma_1$, where ς_1 is the monomer friction coefficient. The random Brownian force $\mathbf{S}(t)$ is assumed to be a Gaussian white noise vector, having the standard properties

$$E\{\mathbf{S}(t)\} = 0, \tag{8a}$$

$$\mathrm{cov}\{\mathbf{S}(t),\mathbf{S}(\tau)\} = 2\varsigma_i k_{\mathrm{B}}T\delta(t-\tau)\mathbf{I}. \tag{8b}$$

The attached end A moves affinely and therefore

$$\frac{\mathrm{d}\mathbf{r}_{\mathrm{A}}(t)}{\mathrm{d}t} = \mathbf{L}(t)\cdot\mathbf{r}_{\mathrm{A}}(t). \tag{9}$$

Using Eqs. (7) and (9), the dynamics of the end-to-end vector of the representative dangling segment may be described by

$$\dot{\mathbf{R}}(t) = \mathbf{L}(t)\cdot\mathbf{R}(t) + \frac{1}{\varsigma_i}(\mathbf{F}(\mathbf{R}(t)) + \mathbf{S}(t)). \tag{10}$$

The convection-diffusion equation for the distribution function of elastic dumbbells with sticky ends was derived by Palierne [32]. Following a similar approach, we formulate the equation for the distribution function of dangling segments in the Fokker-Planck form

$$\frac{\partial\Psi_i^{\mathrm{D}}}{\partial t} = -\frac{\partial}{\partial\mathbf{R}}\cdot\left(\mathbf{L}\cdot\mathbf{R}\Psi_i^{\mathrm{D}} + \frac{1}{\varsigma_i}\mathbf{F}_i(\mathbf{R})\Psi_i^{\mathrm{D}} - \frac{k_{\mathrm{B}}T}{\varsigma_i}\frac{\partial\Psi_i^{\mathrm{D}}}{\partial\mathbf{R}}\right) + g_i(R)(\lambda_i^{\mathrm{D}}\Psi_{i,\mathrm{eq}}^{\mathrm{D}}(\mathbf{R}) - \Psi_i^{\mathrm{D}}(\mathbf{R},t)) - d_i(R)\Psi_i^{\mathrm{D}}(\mathbf{R},t), \tag{11}$$

where $\frac{k_{\mathrm{B}}T}{\varsigma_i}$ is equal to the diffusion constant. The functional forms used for the formation/destruction of dangling segments (attachment/detachment of A-points) are similar to those used in Eq. (6) for bridging segments. Again, it is assumed that the detachment rate of dangling ends is proportional to the current distribution. The attachment is a Brownian process and is proportional to the equilibrium distribution whilst its rate decays during flow. In the next section we discuss the two probability functions $d_i(R)$ and $g_i(R)$.

3. The attachment/detachment dynamics

The problem of adsorption of polymer chains on a solid flat surface in absence of polymer flow was extensively

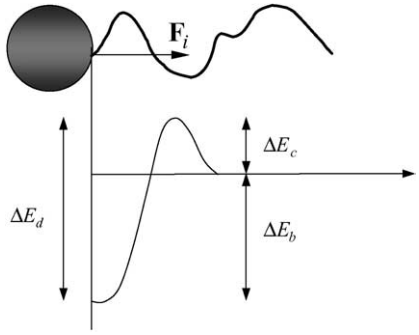

Fig. 3. Schematic representation of the potential energy barrier for detachment of an adsorbed polymer segment from the filler surface.

studied. A comprehensive review of this topic is presented in the monograph by Fleer et al. [37]. In presence of polymer flow, a number of models are proposed for the attachment/detachment dynamics of chains on/from flat surfaces [38–40]. Here we take a view similar to that presented by Chernyak and Leonov [41]. Let us consider an A-point at the end of a macromolecular segment, as shown in Fig. 3. The grafted chain may snap from the nanoparticle either due to thermal fluctuations, or due to the action of the entropic force exerted by the strand. The energy penalty for detachment is ΔE_d, where, for a single strand, $\Delta E_\mathrm{d} = \Delta E_\mathrm{b} + \Delta E_\mathrm{c}$. ΔE_b is the difference between the energy of a bead residing on the surface of the filler and in the bulk polymer. ΔE_c represents the cage barrier for a bead in the dense bulk.

The detachment process is favored by the tension in the strand. This force is represented here by using the Warner approximation to the inverse Langevin function

$$\mathbf{F}_i(\mathbf{R}) = -\frac{3k_\mathrm{B}T}{il^2}\frac{\mathbf{R}}{1-\frac{R^2}{(il)^2}}, \tag{12}$$

where i is the number of beads in the strand and l is the bead-to-bead distance. Then, the detachment rate is given by the Arrhenius form

$$d_i(R) = \tau_0^{-1}\exp\left(\frac{-(\Delta E_\mathrm{d} + F_i(R)\delta)}{k_\mathrm{B}T}\right), \tag{13}$$

where the characteristic time of molecular vibrations, $\tau_0 \sim l\sqrt{\frac{m}{k_\mathrm{B}T}}$, and the activation length δ are constants. The quantity $\tau_i(R) = d_i^{-1}(R)$ represents the average life-time of an attached point (A-point) subjected to stress. Thus, $\tau = \tau_0 \exp\left(\frac{\Delta E_\mathrm{d}}{k_\mathrm{B}T}\right)$ may represent the fundamental relaxation time of the network.

The attachment process may be regarded as the inverse of detachment and is independent of the force in the strand. The energetic penalty for attachment is comparable to the diffusion barrier in the melt and therefore, the attachment rate may be represented by

$$g_i(R) = g_i = \tau_0^{-1}\exp\left(\frac{-\Delta E_\mathrm{c}}{k_\mathrm{B}T}\right). \tag{14}$$

Accordingly, $\tau^* = g_i^{-1}$ represents the average time a bead resides in the 'cage' formed by its neighbors in the bulk polymer. The representative cage in the neighborhood of the filler surface is expected to differ to some extent from the cage in the bulk due to local density fluctuations. This effect is neglected here.

4. Constitutive equation

Both segment types described at Section 2 contribute to stress production. It is assumed that this contribution to the total stress may be expressed as a superposition of contributions of bridging and dangling segments as:

$$\mathbf{T} = \sum_i (\mathbf{T}_i^\mathrm{B} + \mathbf{T}_i^\mathrm{D}), \tag{15}$$

where $\mathbf{T}_i^\mathrm{B}$ and $\mathbf{T}_i^\mathrm{D}$ represent the stress contribution of bridging and dangling strands of length i Kuhn units, respectively. These quantities are evaluated using the virial equation as

$$\mathbf{T}_i^\mathrm{B} = \langle \mathbf{F}_i^\mathrm{B}\mathbf{R}\rangle_\mathrm{B}, \mathbf{T}_i^\mathrm{D} = \langle \mathbf{F}_i^\mathrm{D}\mathbf{R}\rangle_\mathrm{D}. \tag{16}$$

The brackets denote averaging over the respective configuration space, i.e.

$$\langle \mathbf{Q}_i\rangle_j = \int \Psi_i^j \mathbf{Q}_i \mathrm{d}\mathbf{R}. \tag{17}$$

Substituting the expression of the entropic force from (12), the stress tensor reads

$$\mathbf{T} = \frac{3k_\mathrm{B}T}{il^2}\frac{\mathbf{B}_i}{1-\frac{1}{(il)^2}\frac{Tr\mathbf{B}_i}{N_i^\mathrm{B}}} + \frac{3k_\mathrm{B}T}{il^2}\frac{\mathbf{D}_i}{1-\frac{1}{(il)^2}\frac{Tr\mathbf{D}_i}{N_i^\mathrm{D}}}, \tag{18}$$

where

$$\mathbf{B}_i(t) = \int \Psi_i^\mathrm{B}\mathbf{R}\mathbf{R}\,\mathrm{d}\mathbf{R}, \quad \mathbf{D}_i(t) = \int \Psi_i^\mathrm{D}\mathbf{R}\mathbf{R}\,\mathrm{d}\mathbf{R}. \tag{19}$$

In order to evaluate these expressions in close form, a closure approximation similar to that used by Vaccaro and Marrucci [42] is used. The evolution equations for the probability density functions (6) and (11) are multiplied by $\mathbf{RR}$ and the result is integrated over the configuration space. In order to render the expressions tractable, it is assumed that the kinetics depends exclusively on the mean value of the distributions [33,35] and hence, we may replace R^2 for an individual chain with the average value of R^2 taken over the population of the respective type of segments, i.e. with $\frac{Tr\mathbf{B}}{N_i^\mathrm{B}}$ and $\frac{Tr\mathbf{D}}{N_i^\mathrm{D}}$ for the bridges and dangling segments, respectively. With this, the evolution Eqs. (6) and (11)

become

$$\frac{\mathrm{d}\mathbf{B}_i}{\mathrm{d}t} = \mathbf{L}\cdot\mathbf{B}_i + \mathbf{B}_i\cdot\mathbf{L}^{\mathrm{T}} + \xi\tau^{-1}(\lambda_i^{\mathrm{B}}\mathbf{B}_{i,0} - \mathbf{B}_i) - \tau^{-1}\exp\left[\frac{3\sqrt{\frac{Tr\mathbf{B}_i}{N_i^{\mathrm{B}}}}}{il^2\left(1-\frac{\frac{Tr\mathbf{B}_i}{N_i^{\mathrm{B}}}}{(il)^2}\right)}\delta\right]\mathbf{B}_i, \tag{20}$$

$$\frac{\mathrm{d}\mathbf{D}_i}{\mathrm{d}t} = \mathbf{L}\cdot\mathbf{D}_i + \mathbf{D}_i\cdot\mathbf{L}^{\mathrm{T}} + 2\frac{k_{\mathrm{B}}T}{\xi_i}N_i^{\mathrm{D}}\mathbf{I} - \tau_{Ri}^{-1}\frac{1}{1-\frac{\frac{Tr\mathbf{D}_i}{N_i^{\mathrm{D}}}}{(il)^2}}\mathbf{D}_i + \xi\tau^{-1}(\lambda_i^{\mathrm{D}}\mathbf{D}_{i,0} - \mathbf{D}_i) - \tau^{-1}\exp\left[\frac{3\sqrt{\frac{Tr\mathbf{D}_i}{N_i^{\mathrm{D}}}}}{il^2\left(1-\frac{\frac{Tr\mathbf{D}_i}{N_i^{\mathrm{D}}}}{(il)^2}\right)}\delta\right]\mathbf{D}_i, \tag{21}$$

where $\tau_{\mathrm{R}\,i}$ is the Rouse relaxation time of a free chain with i Kuhn units and $\xi = \tau/\tau^*$. As discussed in Section 3, τ and τ^* represent respectively the characteristic time scales for detachment and attachment of chains to the filler in absence of a bias force in the strand.

Similarly, integration of Eqs. (6) and (11), and application of the divergence theorem yields

$$\frac{\mathrm{d}N_i^{\mathrm{B}}}{\mathrm{d}t} = \xi\tau^{-1}(\lambda_i^{\mathrm{B}}N_{i,0}^{\mathrm{B}} - N_i^{\mathrm{B}}) - \tau^{-1}\exp\left[\frac{3\sqrt{\frac{Tr\mathbf{B}_i}{N_i^{\mathrm{B}}}}}{il^2\left(1-\frac{\frac{Tr\mathbf{B}_i}{N_i^{\mathrm{B}}}}{(il)^2}\right)}\delta\right]N_i^{\mathrm{B}}, \tag{22}$$

$$\frac{\mathrm{d}N_i^{\mathrm{D}}}{\mathrm{d}t} = \xi\tau^{-1}(\lambda_i^{\mathrm{D}}N_{i,0}^{\mathrm{D}} - N_i^{\mathrm{D}}) - \tau^{-1}\exp\left[\frac{3\sqrt{\frac{Tr\mathbf{D}_i}{N_i^{\mathrm{D}}}}}{il^2\left(1-\frac{\frac{Tr\mathbf{D}_i}{N_i^{\mathrm{D}}}}{(il)^2}\right)}\delta\right]N_i^{\mathrm{D}}. \tag{23}$$

Eqs. (20)–(23) represent a set of ordinary differential equations in terms of the unknowns $\mathbf{B}_i$, $\mathbf{D}_i$, N_i^{B}, and N_i^{D}. To this set of equations one adds the initial conditions represented by the values of the unknowns at time $t=0$, i.e. $\mathbf{B}_{i,0}$, $\mathbf{D}_{i,0}$, $N_{i,0}^{\mathrm{B}}$, and $N_{i,0}^{\mathrm{D}}$. In addition, the two constants λ_i^{B}, and λ_i^{D} need to be specified.

These parameters are calibrated based on the polymer equilibrium structure obtained from the molecular simulations presented by Ozmusul et al. [29]. The equilibrium distributions for all types of segments, including bridging ($\Psi_i^{\mathrm{B}}(\mathbf{R},0)$), and dangling ($\Psi_i^{\mathrm{D}}(\mathbf{R},0)$), result from the numerical model. Integrating the distributions Eq. (1) one obtains the equilibrium number densities of the two types of segments, $N_{i,0}^{\mathrm{B}}$ and $N_{i,0}^{\mathrm{D}}$. Further, with the aforementioned closure approximation used to evaluate the tensors $\mathbf{B}_i$ and $\mathbf{D}_i$, one obtains

$$B_{11,0} = B_{22,0} = B_{33,0} = \frac{N_{i,0}^{\mathrm{B}}il^2}{3}, \quad D_{11,0} = D_{22,0} = D_{33,0} = \frac{N_{i,0}^{\mathrm{D}}il^2}{3}. \tag{24}$$

Note that in writing these equations it is assumed that the two types of segments are not stretched before loading. In order to evaluate λ_i^{B} and λ_i^{D}, Eqs. (22) and (23) are re-written in equilibrium. They provide a set of two equations for the two constants $\lambda_i^{\mathbf{B}}$ and λ_i^{D} which result as

$$\lambda_i^{\mathrm{B}} = \lambda_i^{\mathrm{D}} = 1 + \frac{1}{\xi}\exp\left[\frac{3\sqrt{i}}{il-l}\delta\right]. \tag{25}$$

The governing equations presented in this section may be solved, in principle, for any flow regime. In the next section we present examples referring to stationary oscillatory and also simple two-dimensional shear flow. In the case of the steady flow, all time derivatives in Eqs. (20)–(23) vanish and the system reduces to a set of algebraic nonlinear equations.

5. Example

A numerical example is considered to demonstrate some of the features of the proposed model. The objective is to evidence the important role played by bridging segments in the overall rheological behavior of nanofilled polymers and to provide a quantitative measure of their effect. This effect is qualitatively observed in experimental studies of polymer mixtures with well-dispersed filler particles [11,15,43,44]. To this end, we examine the steady state response of a nanofilled polymer composite subjected to a two-dimensional shear flow. The equilibrium structure of this system was determined by lattice Monte Carlo simulations in [29]. Here, we review only those details of the simulation procedure and results that are relevant for the present discussion.

The simulation cell is a cube of side length L, which contains spherical impenetrable fillers with radius R_{f} arranged in a simple cubic pattern. Periodic boundary conditions are imposed on all faces of the simulation cell. The volume surrounding the fillers is occupied by a monodisperse population of N_{c} chains of length N links. The simulation is performed for filler volume fractions $\phi = 6$ and 12%. The particle diameter is about twice the chain radius of gyration, while the minimum wall-to-wall distance w equals $1R_{\mathrm{g}}$ and $2R_{\mathrm{g}}$, for the two filler volume fractions, respectively.

The chains are represented as 'pearl necklaces' of spherical beads, each bead representing a Kuhn segment and occupying a lattice site. The chains do not overlap

Table 1
Characteristic parameters used in the Monte Carlo simulations

ϕ (%)	R_f	w	L	N	N_c
6	R_g	R_g	$9R_g$	100	1264
12	R_g	$2R_g$	$11R_g$	100	2550

(excluded volume) and interact with the fillers through a potential that has a stiff repulsive term imposing the non-penetrability condition, and a longer ranged attractive term modeling the polymer–filler affinity. The chains are free to move over a cubic lattice with lattice parameter equal to the inter-bead distance along the chain. The system was equilibrated for several thousand Monte Carlo steps per bead and then chain statistics for the equilibrium structure was collected. Some characteristics of the examined simulation cell are summarized in Table 1.

The distribution functions of bridging, dangling end and loop segments were determined, as well as the total number of these chain segments per filler. The main conclusions of this study are:

1. A wide distribution of polydisperse bridging segments $\Psi^{B}_{i,eq}(\mathbf{R})$ exists. The total number of bridging segments per filler decreases dramatically with the wall-to-wall distance, essentially vanishing when this parameter equals $2R_g$.
2. Dangling ends form a wide distribution $\Psi^{D}_{i,eq}(\mathbf{R})$ including long and short segments. The dangling segments follow approximately a Gaussian distribution of their end-to-end vectors at given i. The distribution depends on the wall-to-wall distance since as the fillers approach each other, part of the long dangling segments become bridges.
3. A large number of loop segments form on the surface of each filler. Their distribution is rather narrow and the loops are short. Their number per filler is independent of the filler wall-to-wall distance and is largely independent of the intensity and range of the attraction between polymers and fillers. The dense population of loops increases the effective filler radius, hence enhancing the hydrodynamic interaction between fillers and matrix at large deformations rates.
4. It was observed that varying the affinity between polymers and fillers has no qualitative effect on the previous conclusions.

This information is used to calibrate the model. In particular, the initial conditions for the model represented by the values of parameters $\mathbf{B}_{i,0}$, $\mathbf{D}_{i,0}$, $N^{B}_{i,0}$, and $N^{D}_{i,0}$ at time

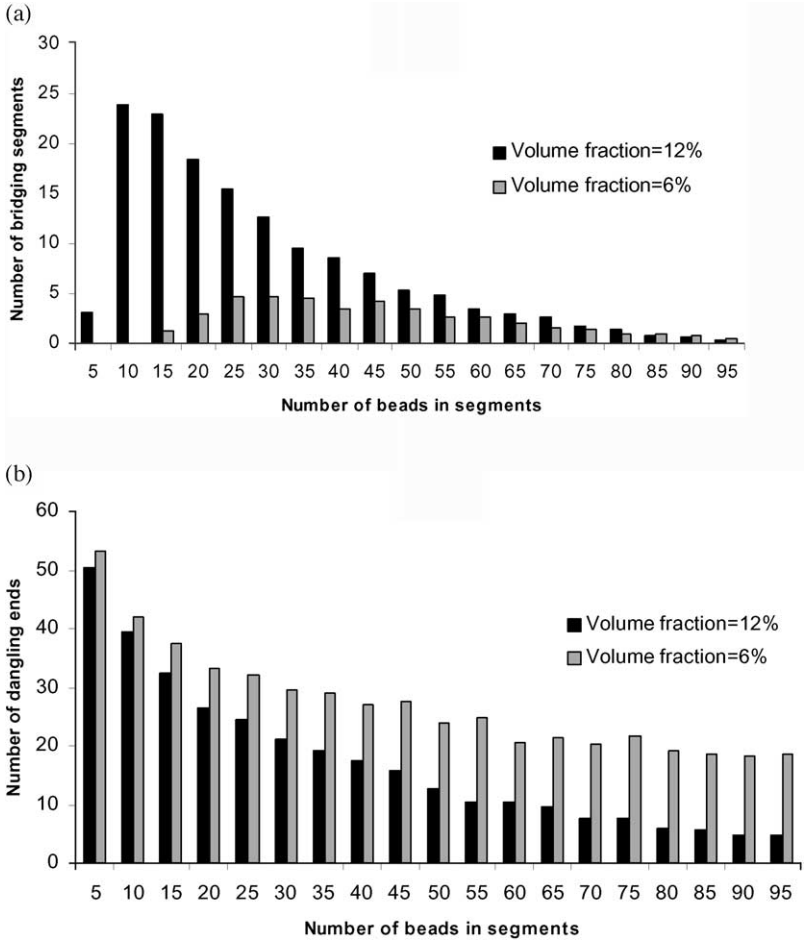

Fig. 4. The number of (a) bridging segments and (b) dangling ends in the simulation box, as determined from discrete simulations (Ref. [29]).

zero are directly derived from the simulation results. Here, in order to simplify the numerical implementation of the model, the actual distributions are considered as piece-wise constant, as shown in Fig. 4(a) and (b). In this particular example, we ignore the contribution of loop segments in stress production, as the number density of long loops is low while the short loop segments are confined to the immediate neighborhood of the wall.

With these initial conditions, as the first example, the model is used to predict the linear dynamic response of the composite subjected to a small amplitude oscillatory shear deformation. Results for overall storage and loss moduli are plotted against normalized frequency $\omega\tau_{RN}$. $\tau_{RN} = 6\varsigma_1 l^2 N^2 / k_B T$ represents the longest Rouse relaxation time of the entire polymer chain with N beads. The Rouse time is taken as the unit of time in this analysis. All lengths are normalized by R_g and the activation length δ is assumed to be on the order of a Kuhn segment. The ratio of the two characteristic times τ and τ^* is taken as $\xi = 10$.

Fig. 5 shows the variation of the storage modulus $G'(\omega)$

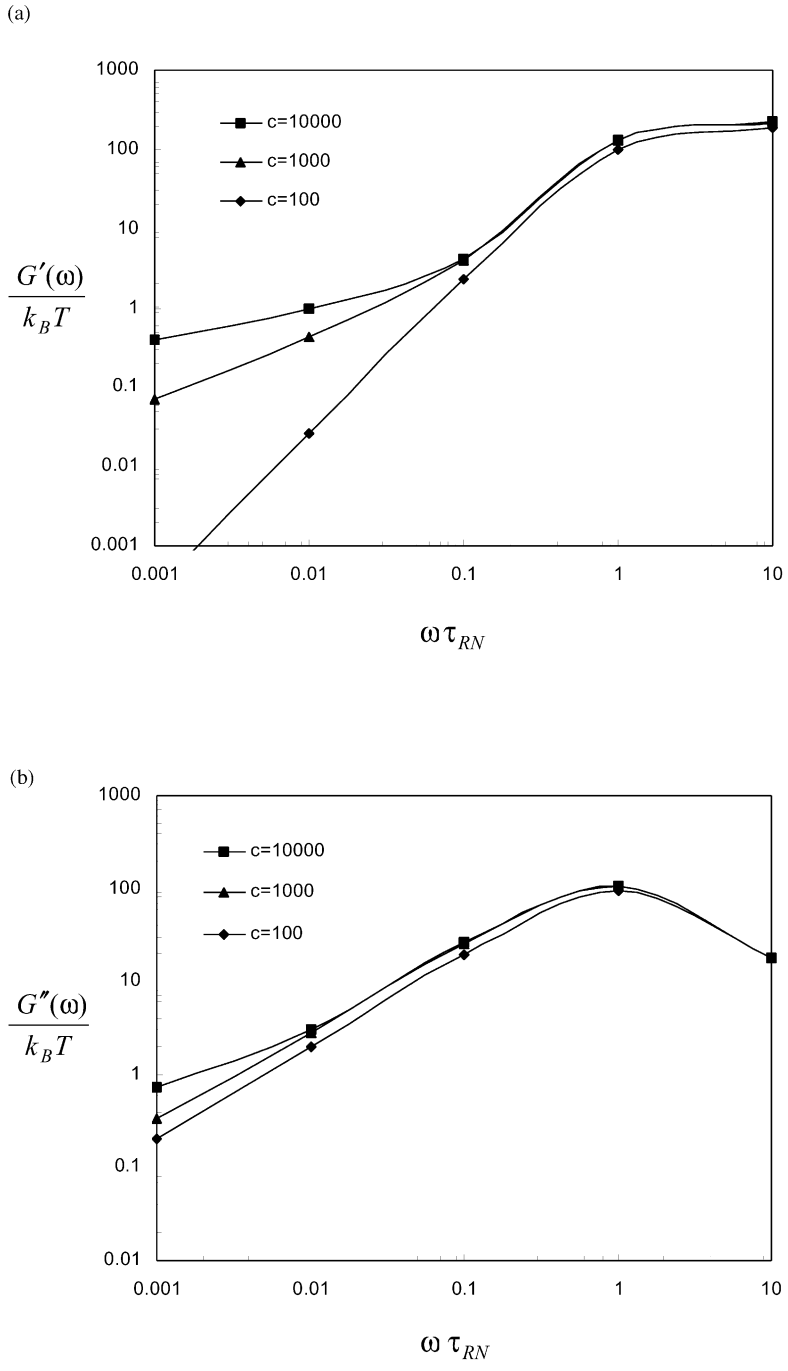

Fig. 5. Storage (a) and loss (b) moduli for three nanofilled polymer systems at constant filler volume fraction (12%) and different energetic polymer–nanoparticle interaction.

and loss modulus $G''(\omega)$ in a frequency sweep for composites having filler concentration (12%, wall-to-wall distance R_g) and different polymer–filler affinity. Here, the parameter c is defined as the ratio of the lifetime of A-points, τ, to the Rouse relaxation time τ_{RN}. When the filler–polymer interaction is weak, the typical slopes of the neat polymer, equal to 2 and 1 for $G'(\omega)$ and $G''(\omega)$, respectively, are obtained at low frequencies. The solid-like plateau at frequencies higher than τ_{RN}^{-1} is due to the fact that no relaxation modes faster than the Rouse relaxation are included in the model. Although possible, this was not attempted since the focus here is on the long relaxation time associated with the polymer–filler interaction.

As the parameter c increases, a terminal plateau region forms indicating a transition from liquid to solid like behavior once stress relaxation is effectively hindered by the presence of nanoparticles. The transition is more obvious in the storage modulus $G'(\omega)$ than in $G''(\omega)$. This slowdown at low frequencies is observed experimentally in nanocomposites when the filler volume fraction and filler size favor the

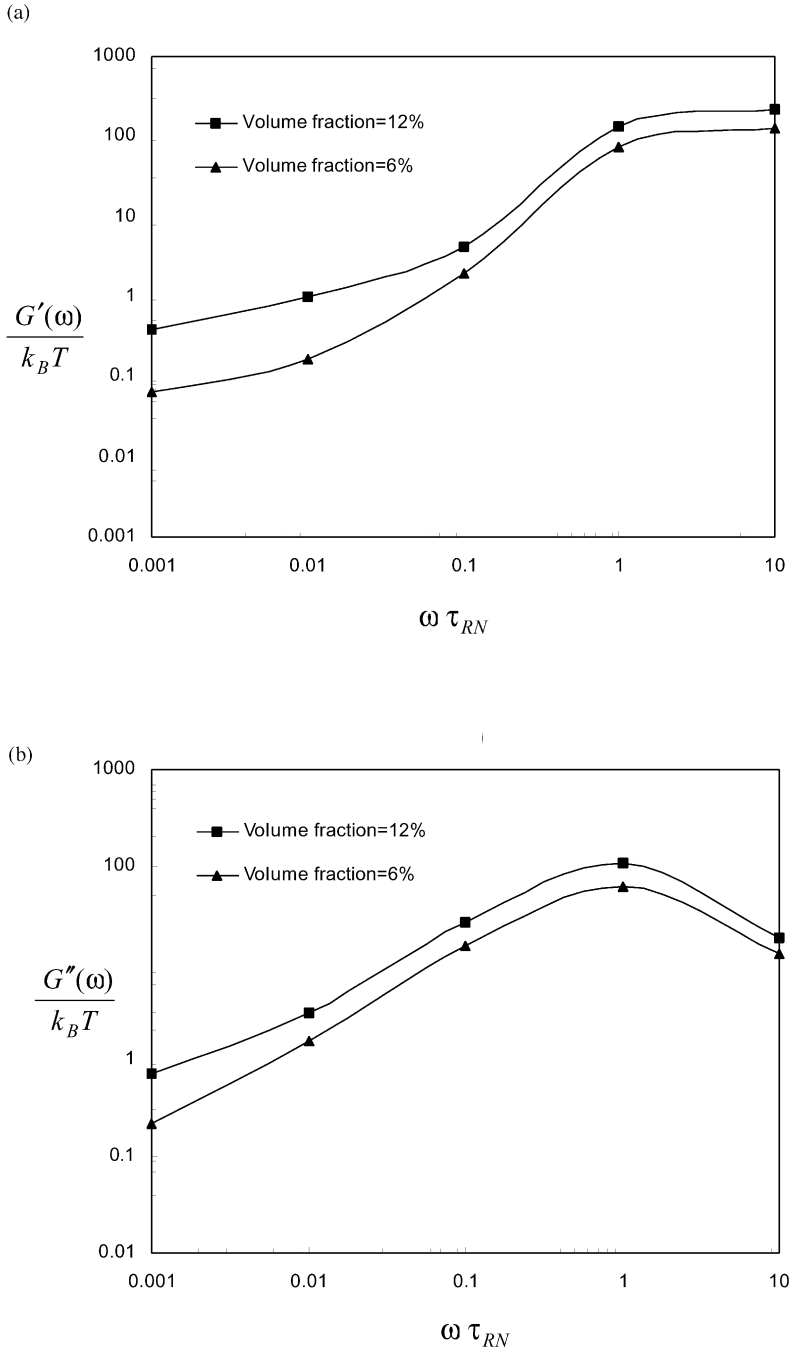

Fig. 6. Frequency response of nanofilled polymer systems at different filler volume fraction ($\phi = 6$, 12%) with constant energetic polymer–nanoparticle interaction ($c = 10{,}000$). (a) Storage modulus $G'\omega$; (b) loss modulus $G''\omega$.

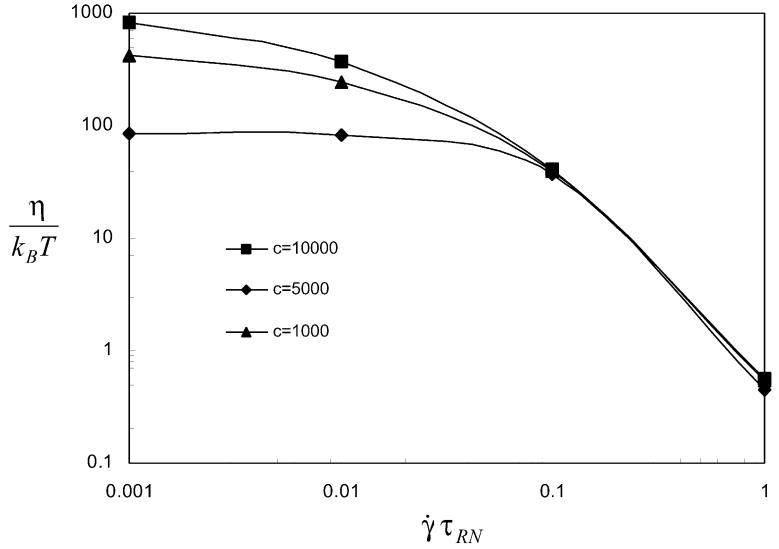

Fig. 7. The shear viscosity vs. non-dimensional velocity gradient for three polymer–filler affinities described by the ratio $c=10{,}000$, 5000, and 1000. The concentration of filler particles is 12%.

formation of a bridging polymer network [11,15,44]. The effect is similar to that induced by cross-links in rubbers. Here, the polymer–filler attachment points play a role equivalent to that of the cross-links.

The frequency sweeps for $G'(\omega)$ and $G''(\omega)$ at two different filler concentrations are shown in Fig. 6. Here, the affinity parameter is kept constant at $c=10{,}000$. We have ignored any contribution of hydrodynamic interactions and thus, the observed increase in dynamic linear response with filler volume fraction is due solely to the increase of the number density of bridging segments.

Further, the stationary shear viscosity (η) of the reinforced melts with different polymer–particle interaction and filler concentrations was investigated. The results are shown in Figs. 7 and 8. A well-defined zero-shear rate plateau is observed at low velocity gradient ($\dot{\gamma}$) in all cases. The viscosity in this Newtonian range is due entirely to the effect of the bridge detachment and re-attachment process. In order to accommodate the imposed strain, detachment of bridging and dangling segments occurs at all strain rates. At low imposed strain rates, the rate of re-attachment is high enough such that the population of bridges and dangling segments is essentially constant during deformation. Since the structure remains stationary, the viscosity is rate independent under such conditions. The plateau is sensitive to the lifetime of the A-points and increases almost linearly with τ (Fig. 7).

At higher shear rates, the model reproduces a shear thinning behavior, which is controlled mainly by the kinetics of chain detachment from fillers. The polymer–filler detachment rate is higher than the rate of attachment in fast

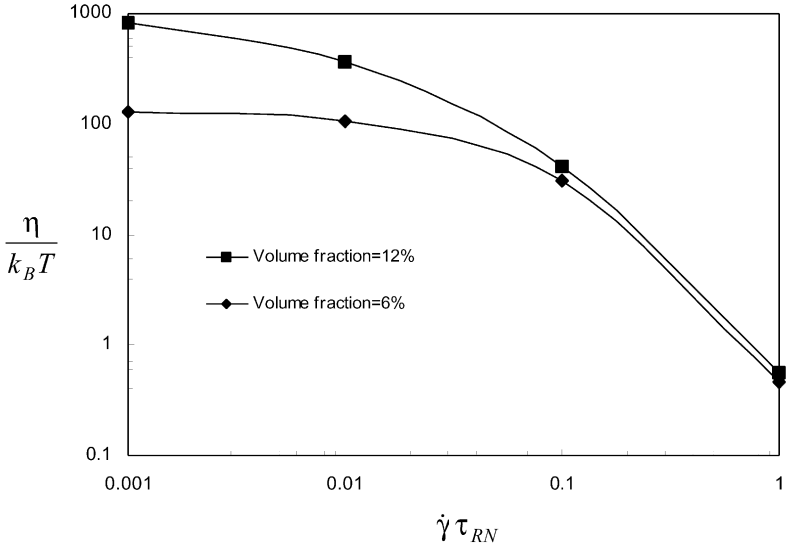

Fig. 8. The shear viscosity vs. non-dimensional velocity gradient at two polymer–filler concentration $\phi=6$, 12%. The average lifetime of A-points is kept constant at $c=10{,}000$.

flows. This leads the development of a yield stress for the filled fluid and to the onset of nonlinear viscoelasticity. In this range the contribution of bridging segments becomes negligible and viscosity is associated with the large population of dangling ends. Since the influence of hydrodynamic interactions is not captured in the present formulation, the model cannot be applied to the very high shear rates regime.

6. Conclusions

A molecular network model describing the viscoelasticy of polymer-based nanocomposite is presented. A material with significant energetic interactions between polymers and fillers and with well-dispersed fillers is considered. The fillers have low concentration (on the order of 10 vol.%) and small dimensions, with their diameter being on the order of two polymer gyration radii. The high affinity of polymers to fillers leads to the formation of polymer–filler junctions. Under these particle size and volume fraction conditions, the wall-to-wall distance between fillers is small and polymeric chains bridge neighboring fillers and form a network of nanoparticles and adsorbed macromolecules. The kinetics of this network is represented within the framework of the traditional transient network theories. The contribution of the dangling ends is accounted for by using an elastic dumbbell model. The evolution of the internal structure during deformation is represented by a set of diffusion-convection equations. The material structure was determined from atomistic simulations of the filled system, which provide the initial conditions for the evolution equations. Several features of the model were demonstrated for applied steady and oscillatory shear deformation. It is observed that, to a large extent, the overall material viscoelasticity can be controlled by the lifetime of filler–polymer junctions. Consistent with experimental observations, the model exhibits the transition to rubber-like behavior at low frequencies in case of very strong filler–polymer interactions. It also exhibits constant viscosity at low strain rates and shear thinning response in fast flows.

Although the model described here captures several essential features of the molecular structure and its evolution during deformation, it has few notable limitations. Some assumptions made were tested by atomistic simulations, while others remain purely phenomenological. For example, it was assumed that the stress production in the two networks is purely additive and there is no stress transfer between them. This assumption is expected to be valid as long as the filler distribution and therefore the network of bridging segments are spatially uniform. Other limitations of the model include the omission of the hydrodynamic interactions which are expected to be important in fast flows and at large deformations, and the fact that the model does not capture the conversion of one type of segment into another as the structure evolves (e.g. upon failure of an *A*-point, a bridge transforms into a dangling end).

Acknowledgements

We are grateful to Prof. J.F. Palierne for his valuable comments on the general theory of transient networks. One of the authors, C.R. Picu, acknowledges the support of the US Office of Naval Research through grant N00014-01-1-0732. He also thanks Prof. S. Kumar and Mr. M.S. Ozmusul for providing access to the molecular simulations results.

References

[1] Medalia A. J Colloid Interface Sci 1970;32:115.
[2] Frolich J, Goritz D. Kautsch Gummi Kumstst 1998;51:370.
[3] Piau JM, Dorget M, Palierne JF, Pouchelon A. J Rheol 1999;43:305.
[4] Kohl DJ, Beaucage G. Curr Opin Solid State Mater Sci 2002;6:183.
[5] Rehner J. In: Kraus G, editor. Reinforcement of elastomers. New York: Interscience; 1965. p. 153.
[6] Leblanc J. J Appl Polym Sci 1997;66:2257.
[7] Wang M. Rubber Chem Tech 1998;71:521.
[8] Wattenbarger MR, Chan HS, Evans DF, Bloomfield VA, Dill KA. J Chem Phys 1990;93:8343.
[9] Picu RC, Ozmusul MS. J Chem Phys 2003;118:11239–48.
[10] Payne AR. In: Kraus G, editor. Reinforcement of elastomers. New York: Interscience; 1965. p. 69.
[11] Aranguren MI, Mora EM, DeGroot JV, Macosko CW. J Rheol 1992; 36:1165.
[12] Cassagnau P, Mélis F. Polymer 2003;44:6607.
[13] Simhambhatla M, Leonov AI. Rheol Acta 1995;34:329.
[14] Montes H, Lequeux F, Berriot J. Macromolecules 2003;36:8107.
[15] Havet G, Isayev AI. Rheol Acta 2003;42:47.
[16] Metzner AB. J Rheol 1985;29:739.
[17] Poslinski AJ, Ryan ME, Gupta RK, Seshadri SG, Frechette FJ. J Rheol 1988;(32):704.
[18] Bossis G, Brady JF. J Chem Phys 1989;91:1866.
[19] Huber G, Vilgis TA. Macromolecules 2002;35:9204.
[20] Heinrich G, Klüppel M. Adv Polym Sci 2002;160:1.
[21] Leonov AI. J Rheol 1990;34:1039.
[22] Havet G, Isayev AI. Rheol Acta 2001;40:570.
[23] Maier PG, Göritz D. Kautsch Gummi Kumstst 1996;49:18.
[24] Solomon M, Lu Q. Curr Opin Solid State Mater Sci 2001;6:430.
[25] Picu RC, Ozmusul MS. Polymer 2002;43:4657.
[26] Picu RC, Sarvestani AS, Ozmusul MS. In: Harik VM, Luo LS, Salas MD, editors. Trends in nano-scale mechanics. Dordrecht: Kluwer Academic Press; 2003. p. 61.
[27] Brown D, Mélé P, Albérola ND. Macromolecules 2003;36:1395.
[28] Sharaf MA, Kloczkowski A, Mark JE. Comput Theor Polym Sci 2001;11:251.
[29] Ozmusul MS, Picu, RC, Kumar, S. 2004 to be submitted.
[30] Doremus P, Piau JM. J Non-Newtonian Fluid Mech 1991;39:335.
[31] Bird RB, Armstrong RC, Hassager O., 2nd ed Dynamics of polymeric liquids, vol. 2. New York: Wiley; 1987.
[32] Palierne JF. Rheol Acta 1997;36:534.
[33] Phan Thien N, Tanner RI. J Non-Newtonian Fluid Mech 1977;2:353.
[34] Lodge AS. Trans Faraday Soc 1956;52:120.
[35] Mewis J, Denn MM. J Non-Newtonian Fluid Mech 1983;12:69.
[36] De Kee D, Fong CM. Polym Engng Sci 1994;4:438.

[37] Fleer GJ, Cohen Stuart M, Scheutjens J, Cosgrove T, Vincent B. Polymers at interfaces. London: Chapman and Hall; 1993.
[38] Ajdari A, Brochard-Wyart F, de Gennes PG, Leibler L, Viovy JL, Rubinstein M. Physica A 1994;204:17.
[39] Hatzikiriakos SG, Kalogerakis N. Rheol Acta 1994;33:38.
[40] Yarin AL, Graham MD. J Rheol 1998;42:1491.
[41] Chernyak YB, Leonov AI. Wear 1986;108:105.
[42] Vaccaro A, Marrucci G. J Non-Newtonian Fluid Mech 2000;92:261.
[43] Sternstein SS, Zhu AJ. Macromolecules 2002;35:7262.
[44] Zhang Q, Archer LA. Langmuir 2002;18:10435.